Microgravity Sci. Technol. (2012) 24:255–265
DOI 10.1007/s12217-012-9308-7

ORIGINAL ARTICLE

Numerical Simulation of Nucleate Boiling Phenomenon Coupled with Thermal Response of the Solid

Eduardo Aktinol · Vijay Kumar Dhir

Received: 22 November 2011 / Accepted: 7 May 2012 / Published online: 6 June 2012

Abstract The present work describes the response of a heated solid surface during nucleation, growth and departure of a single bubble. Two dimensional, axisymmetric, finite difference schemes are used to solve the governing equations in the liquid, vapor and solid phases. The interface between liquid and vapor phases is tracked by a level set method. An iterative procedure is used at the interface between the solid and fluid phases in order to match temperatures and heat fluxes. Time and space invariant heat fluxes are supplied at the solid base and calculations are carried out for solids with different thermo-physical properties and thicknesses. Near the three-phase contact line, temperatures in the solid are observed to fluctuate significantly over short periods as the bubble base first expands outwards then contracts inwards before departure. The results show that waiting and growth periods can be related directly to wall superheat. The functional relationship between waiting time and wall superheat is found to agree well with the correlations based on experimental data reported in the literature.

Keywords Nucleate boiling · Numerical simulation · Conjugate conduction

Nomenclature

c_p	thermal capacity
f	bubble release frequency
g	gravity vector
h	grid spacing
k	thermal conductivity
L	thickness of solid
q	heat flux
r	radial coordinate
R	radial size of domain
t	time
T	temperature
y	vertical coordinate
Y	vertical size of domain
α	thermal diffusivity
δ	boundary layer thickness
ρ	density

Subscripts

0	characteristic value
d	departure
e	earth
g	growth
l	liquid
ref	reference value
s	solid
v	vapor
w	waiting or wall

Introduction

Nucleate boiling is a process characterized by a liquid-vapor phase change on a heated solid surface. Due to the complexity of the phenomena involved in this highly efficient heat transfer process, a fully mecha-

E. Aktinol · V. K. Dhir (✉)
Henry Samueli School of Engineering and Applied Science, Department of Mechanical and Aerospace Engineering, University of California, Los Angeles, CA 90095, USA
e-mail: vdhir@seas.ucla.edu

nistic model has not yet been established. Nevertheless, with the contributions of approximate models, empirical correlations, and numerical simulations, great strides have been made towards a fundamental understanding of bubble nucleation and growth on heated solid surfaces.

Son et al. (1999) performed numerical simulations and experiments to study the dynamics and heat transfer associated with a single bubble during nucleate boiling on a horizontal surface. The simulated bubble growth and departure processes were found to agree with experimental results to a high degree of accuracy. With an entirely different approach, Yoon et al. (2001) performed simulations of the single bubble dynamics phenomenon and also obtained experimentally confirmed results.

However, one of the key assumptions that both numerical models share is that the surface temperature is constant in time and uniform in space, thereby completely ignoring the thermal response of the solid surface. This is likely to influence the cyclic behavior of bubble evolution, growth and departure processes. Furthermore, with the constant temperature assumption, the waiting time between successive nucleation of bubbles at a given site cannot be determined and must be specified empirically. This deprives the simulation from being able to predict the dependency of waiting time on wall superheat. Consequently, the prediction of heat transfer rates for various boiling regimes where the waiting time would not remain fixed is severely limited unless waiting time is specified empirically.

Moore and Mesler (1961) showed experimentally that wall temperature fluctuations can be significant during nucleate boiling. Also, in addition to the investigation of local temperature fluctuations, there have been experimental efforts to study the influence of the wall's thermal properties on nucleate boiling heat transfer. Magrini and Nannei (1975) studied the effects of both the wall thickness and the thermal properties of different solids on nucleate boiling. They concluded that both parameters strongly influence nucleation site density and therefore heat transfer.

Guo and El-Genk (1994) developed a numerical model based on microlayer evaporation that likewise predicts a strong influence of the wall's thickness and thermal properties on initial bubble growth rates. More recently, Mann et al. (2000) conducted numerical simulations of a single bubble with a wedge-shaped micro region to study the influence that heat conduction in the wall has on nucleate boiling heat transfer. However, in both simulations, the contribution of the induced convection due to bubble growth and detachment is neglected. Likewise, quasi-stationary heat transfer is assumed which results in unrealistic estimates of bubble growth and heat transfer.

Kunkelmann and Stephan (2010) performed transient numerical simulations that included the heat transfer between the fluid and solid phases. The authors showed the spatial variation in surface temperature and heat transfer rates but chose to impose the waiting time based on experimental values.

The objectives of this study are to perform complete simulations of bubble dynamics on a single nucleation site coupled with the thermal response of the supporting horizontal surface and to quantify the dependency of the waiting time, growth period, and heat transfer on the wall's thermal properties, thickness, and nucleation superheat.

Numerical Model Development

Following the work of Son et al. (1999), the computational domain on the fluid side is first divided into micro and macro regions. As seen in Fig. 1, the micro region contains the thin liquid film that forms between the bubble and the solid surface. The liquid film thickness varies from the order of the size of a molecule to the mesh size. The solution for the microlayer is obtained separately by solving the conservation equations to obtain the dependence of film thickness and heat flux on radius. Thus, by splitting the domain, the microlayer can be accounted for without stringent restrictions on mesh size. The macro region contains the rest of the domain including the saturated liquid and the vapor space. The solid wall region under the fluid side computational domain is treated separately.

All processes are assumed to be axisymmetric and flow is assumed to be laminar. The fluid and solid properties including density, thermal conductivity, and viscosity are all assumed to be constant in each phase. The effect of temperature on surface tension is included in the solution of the microlayer. The interface between the liquid and vapor phases is tracked by a level set method modified by Son et al. (1999) to accommodate the effect of phase change. An iterative procedure is used at the interface between the solid and fluid phases in order to match temperatures and heat fluxes on the fluid and solid sides.

For details about the numerical formulation in the microlayer, refer to Lay and Dhir (1995) and Son et al. (1999). In the fluid region, the numerical formulation for all the governing equations as well as the level set solution is outlined by Son et al. (1999, 2002) with only minor changes to the boundary conditions used and the order in which the solution is carried out. Also, the temperature inside the bubble is no longer assumed to

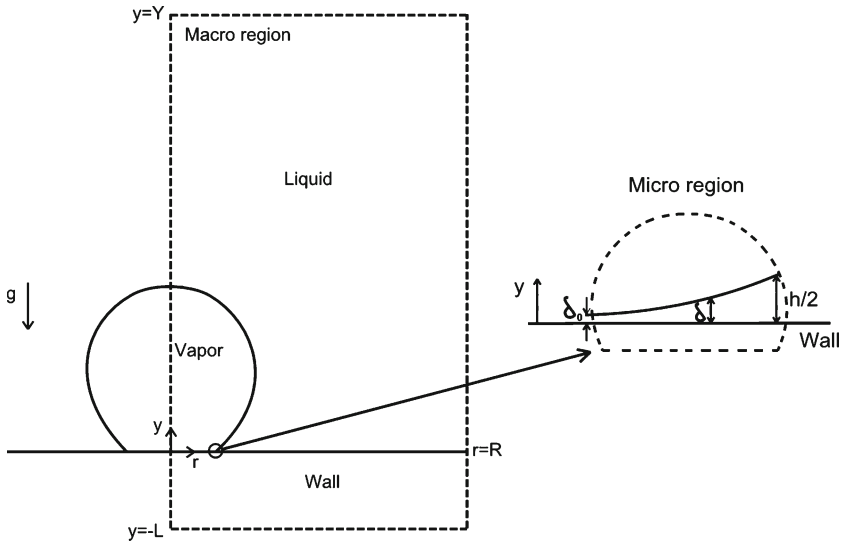

Fig. 1 Different regions of the computational domain used in the simulations

remain constant at saturation temperature. The energy equation is solved throughout the computational domain and a temperature distribution is obtained on the vapor side as well.

Inside the solid wall, the phenomenon of interest is transient conduction. The axisymmetric energy conservation equation in cylindrical coordinates for the solid can be written as

$$\rho c_{ps} \frac{\partial T}{\partial t} = k_s \left[\frac{1}{r} \frac{\partial}{\partial r} \left(r \frac{\partial T}{\partial r} \right) + \frac{\partial^2 T}{\partial y^2} \right] \tag{1}$$

Numerous well-established methods are available to solve this type of equation. For simplicity of implementation without sacrificing speed, accuracy, or stability, an alternating-direction implicit (ADI) method was used. This results in a two step solution procedure in which each step requires the solution of a separate tridiagonal matrix. This is accomplished using the also well-established Thomas algorithm.

Equation 1 is first discretized using the Crank-Nicolson scheme for second order accuracy in both time and spatial directions. The discretized equation is then factorized and rewritten in two steps following the general method developed by Douglas and Gunn (1964).

Physically, at the inner boundary which corresponds to the origin of the domain, the temperature gradient must be zero due to the axisymmetric assumption. At the outer radial boundary, perfect insulation is assumed. In both cases the gradient of the temperature can be written as

$$\frac{\partial T}{\partial r} = 0 \quad \text{at} \quad r = 0, R \tag{2}$$

At the bottom boundary, for a realistic simulation, a constant heat flux is applied such that

$$k \frac{\partial T}{\partial y} = constant \quad \text{at} \quad y = -L \tag{3}$$

The only complication that arises from the addition of the solid wall to the simulation is the boundary between the solid and the fluid. This boundary condition is not only required in order to run the simulation, it is also an area of interest because the surface of the solid is where the highest temperature fluctuations are expected.

Initially, the fluid-side energy equation is solved assuming a constant wall temperature at the lower boundary of the computational domain in the liquid. Using that temperature boundary condition and the newly-solved temperature distribution inside the liquid, a heat flux into the fluid can be calculated from the definition of the heat flux

$$q\,(r, t) = -k \frac{\partial T}{\partial y} \quad \text{at} \quad y = 0 \tag{4}$$

Once this heat flux is calculated, the energy conservation equation for the solid wall is solved using this heat flux at the upper boundary surface. A new temperature field is thus obtained inside the solid, and a new temperature boundary condition is available for use on the fluid side. In order to ensure that energy is conserved at the interface between the wall and the fluid at every time step, this procedure is repeated until both temperatures and heat fluxes display insignificant change between iterations such that the temperature is continuous in all phases and the heat flux going out of the solid matches exactly the heat flux going into the fluid. Once this is accomplished, the calculations will proceed to the next time step.

Although the boundary conditions are physically and mathematically simple, their implementation into the ADI scheme is not straightforward because of the time step splitting. In order to maintain second order accuracy in time, the procedure developed by Zeng and Zhu (2002) is employed when implementing the temperature boundary conditions at the fractional time step. This procedure relies on an additional layer of ghost points on each side of the boundary and on the commutative property of the central difference operators.

Results and Discussion

All simulations were performed using the properties of saturated water at one atmosphere pressure. With those properties, characteristic length, velocity, and time were defined as follows:

$$\begin{aligned} l_0 &= \sqrt{\frac{\sigma}{g\,(\rho_l - \rho_v)}} \\ u_0 &= \sqrt{g l_0} \\ t_0 &= \frac{l_0}{u_0} \end{aligned} \tag{5}$$

The governing equations on the fluid side were normalized with the above determined characteristic quantities. A static contact angle was used and specified to be 35°. The computational domain on the fluid side was chosen to be $(R/l_0, Y/l_0) = (1, 4)$. This affords a compromise between being small enough to allow for practical computational time but large enough that the simulations are unaffected by the boundaries. Initially, there is no bubble present and the liquid is assumed stationary and saturated everywhere except for a thermal boundary layer with linear temperature gradient adjacent to the wall.

On the solid side similar characteristic quantities were defined.

$$\begin{aligned} l_{0s} &= L \\ t_{0s} &= \frac{\alpha_s}{l_0^2} \\ \Delta T_{ref} &= \frac{T - T_{sat}}{T_{ref} - T_{sat}} \end{aligned} \tag{6}$$

Assuming that the initial rate of heat removal from the wall matches exactly the heat input and that the initial surface temperature of the wall ΔT_{ref} is uniform, the initial linear boundary layer thickness is evaluated. The temperature distribution in the solid wall is initially calculated assuming steady state conduction between the applied heat flux at the base of the heated surface and the uniform surface temperature ΔT_{ref}. This produces a uniform temperature distribution inside the solid, at which point a bubble is placed at the origin of the domain. For every subsequent cycle, the nucleation criterion used to determine when to place an embryo at the origin is the temperature of the surface at the cavity site. When that temperature reaches ΔT_{ref} a bubble embryo is placed over the cavity. The simulation then proceeds through several cycles until no more changes can be observed between each cycle.

There are different theories available to predict the temperature at which nucleation occurs. Most often these depend on cavity size and surface wettability of the liquid-solid combination. The choice of nucleation temperature was based on the study of gas entrapment performed by Wang and Dhir (1993) and the effect of surface wettability on active nucleation site density, also by Wang and Dhir (1993).

Figure 2, shows the heat flux at the surface as the simulation proceeds from initial to quasi steady-state conditions. The first noticeable effect of the application of a constant heat flux boundary condition is that as the cycles evolve the waiting time changes before reaching a steady value. This is simply due to the uncertainty in the specification of initial conditions. The area- and cycle-averaged wall heat flux also varies slightly before settling at the same value as the input heat flux. The behavior observed in Fig. 2 indicates that initially the solid is actually being heated as the input heat flux is higher than the area- and cycle-averaged output. Eventually, the output becomes larger than the input and the wall cools back down before reaching a cycle-to-cycle steady value that is equal to the input value.

A plot of the temperature field during bubble growth is shown in Fig. 3a and b along with the vapor-liquid,

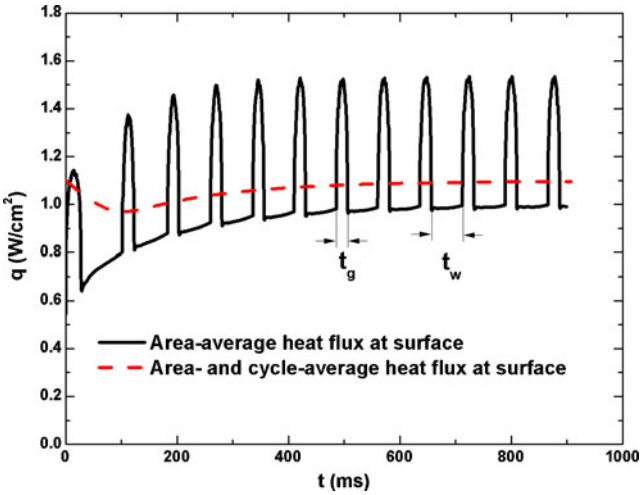

Fig. 2 Variation of heat flux with time for various bubble cycles using a 1 mm thick steel plate and constant $q_{w,in} = 1.1$ W/cm^2 with $\Delta T_{ref} = 6$ K at one atmosphere pressure

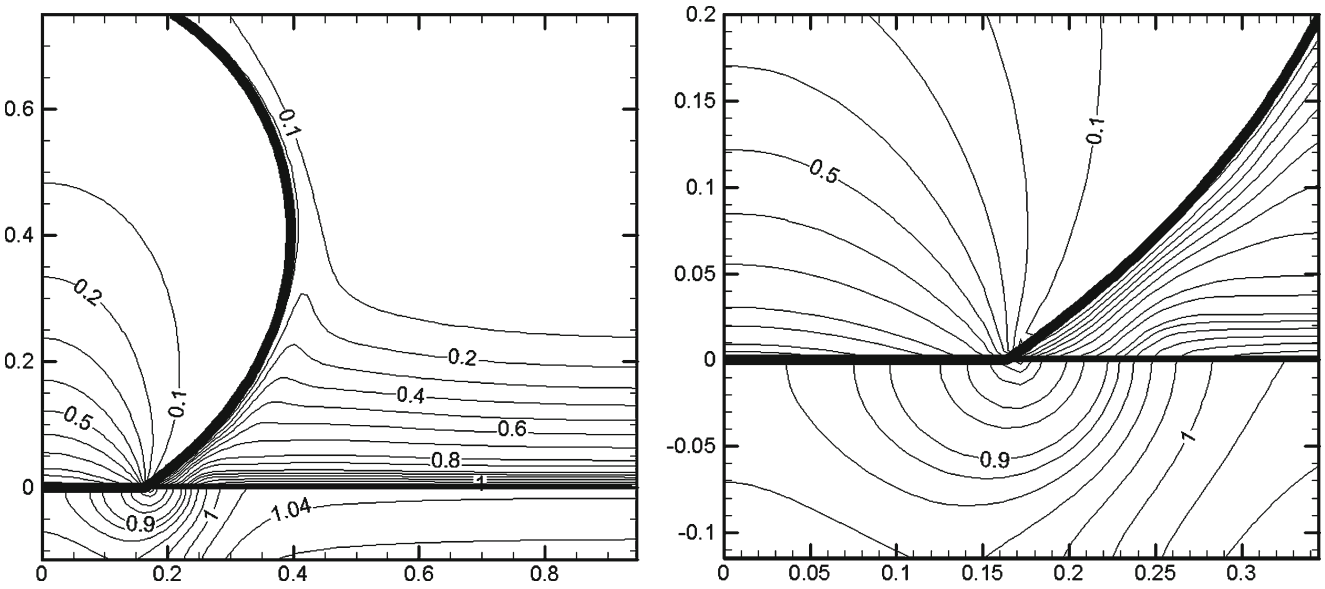

Fig. 3 Temperature contours and phase interfaces for water boiling on a steel disc of 0.3 mm thickness at one atmosphere pressure, $q_{w,in} = 1.1$ W/cm^2 with $\Delta T_{ref} = 6$ K

liquid-solid, and solid-vapor interfaces for water boiling on a smooth 0.3 mm thick stainless steel disc with a single cavity at one atmosphere pressure. In Fig. 3b, a close-up of the area of interest is shown. It can be clearly seen from the temperature contours that the temperature drop in the solid is most pronounced at the point where the bubble interface comes into contact with the wall. This is where the microlayer is located and where significant evaporation takes place. Thus, the three-phase point is the approximate location with the highest rate of heat removal from the solid wall. Elsewhere on the surface of the wall, the phase change phenomenon affects the heat transfer only indirectly due to fluid motion induced by growth and departure of bubbles.

Referring back to Son et al. (1999), the effect of specification of constant heat flux condition at the back side of the solid wall on the bubble dynamics and heat transfer can be quantified. For this comparison, the case with a 0.5 mm thick stainless steel coupled solid substrate was simulated first due to the fact that both the wall superheat and the waiting period are required inputs for running the constant wall temperature case and neither can be anticipated exactly. Since the wall superheat varies both in time and space, the quantity reported is averaged over the entire radius of the computational domain, $R = 2.5$ mm at the surface of the wall and over the span of a full ebullition cycle which includes both the growth and waiting periods.

$$\Delta T_w = \frac{1}{R^2\left(t_g + t_w\right)} \int_{t=0}^{t=t_g+t_w} \int_{r=0}^{r=R} \frac{T - T_{sat}}{\Delta T_{ref}} \, r \, dr dt \quad (7)$$

Using the calculated wall superheat and waiting period, the case with constant wall superheat was simulated to match the conditions as closely as possible. The results listed in Table 1 show that for identical average wall superheats, the rate of heat removal from the wall is approximately seven percent higher in the constant wall superheat case. This indicates that the presence of the wall temperature fluctuations tend to slightly reduce the efficacy of the boiling process. Therefore, a wall that is artificially kept at a constant superheat slightly over-predicts the rate of heat removal and the assumption of constant wall temperature to study bubble dynamics is not unrealistic.

Figure 4 shows the temperature fluctuations at the surface of the solid as a function of time for both the present study and the experimental findings of Moore and Mesler (1961). The experiments were run for high heat flux, fully developed nucleate boiling on a 1.6 mm nichrome strip, whereas the present study focuses on single cavity, isolated bubble cycles on a 1 mm thick steel surface. Both the thermal conductivity

Table 1 The effect of boundary conditions on heat transfer and bubble dynamics for a 0.5 mm thick stainless steel plate with $\Delta T_{ref} = 6$ K

	Constant q_w	Constant ΔT_w
ΔT_w (K)	6.52 (outcome)	6.52 (imposed)
D_d (mm)	2.47	2.57
t_g (ms)	19.8	19.3
q_w (W/cm^2)	1.10 (imposed)	1.18 (outcome)
T_w (ms)	67.1 (outcome)	67.1 (imposed)

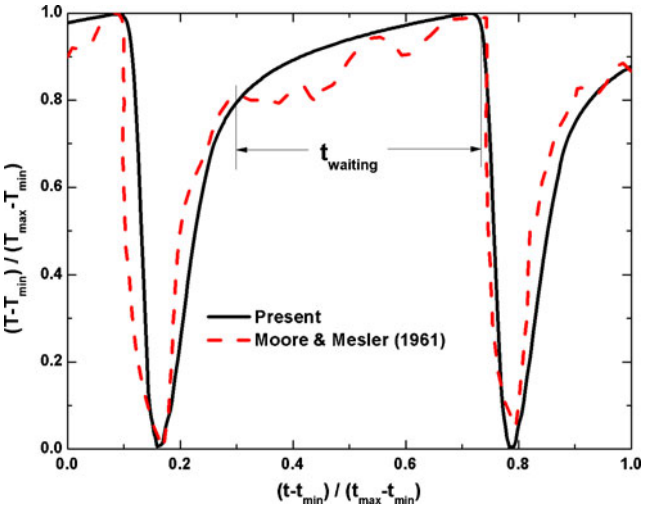

Fig. 4 Comparison between numerical and experimental wall surface temperature fluctuations in time for a fixed radial location. The experiments were run on 1.6 mm nichrome at high heat flux fully developed nucleate boiling and the maximum temperature drop is approximately 15 K. The numerical simulations are for low heat flux single bubbles on a 1 mm steel surface and the maximum temperature drop is approximately 5 K.

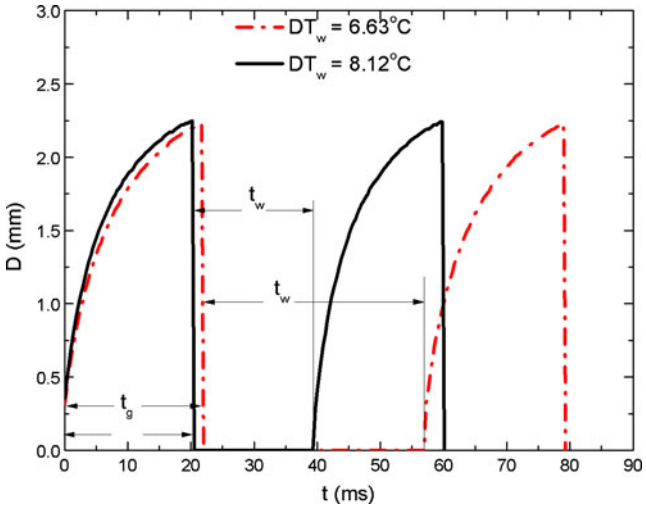

Fig. 5 Effect of wall superheat on growth and waiting time for water boiling on a 1 mm thick copper disc at one atmosphere pressure and two different input heat fluxes $q_{w,in} = 1.1$ W/cm^2 and $q_{w,in} = 1.5$ W/cm^2

and diffusivity of steel are approximately 15% higher than those of nichrome. In the experiments, observed temperature drops at the location of the embedded thermocouple exceeded 15 K and the time elapsed between successive cycles was as low as 10 ms. The location monitored in the present study is 0.4 mm away from the center of the cavity, approximately where the bubble base diameter reaches its maximum. In the simulations the temperature drops rarely exceed 5 K for a steel surface with $\Delta T_{ref} = 6$ K. Therefore, in order to compare the present study with the experimental results of Moore and Mesler (1961), the wall superheat and the time are normalized such that the graph shows two cycles and the entire temperature range for both cycles. Although the wall superheats in the two cases are different, the overall behavior observed is very similar. At the surface of the solid, temperatures fluctuate noticeably over short periods as the bubble base first expands outwards then contracts inwards before departure.

Due to the sharp heat flux peak approximately accompanying the triple point (as shown later in Fig. 11) when the bubble base diameter reaches the monitored location the temperature drop is sharp. As the base diameter shrinks, the wall temperature rises. However, after the bubble ultimately departs, although the heat transfer is no longer aided by the evaporation of the microlayer, the wall is kept cool by the liquid that rushes in to replace the volume previously occupied by the bubble and the remaining temperature recovery is much slower as heat diffuses into the liquid. This phenomenon of transient reheating of the liquid thermal layer directly above a cavity site is usually referred to as 'transient conduction' and has been studied by different authors in an attempt to model the waiting time between successive bubble nucleations. Hsu and Graham (1961, 1986) and Han and Griffith (1965) approximated it as one-dimensional transient conduction in a slab. This behavior has also recently been observed

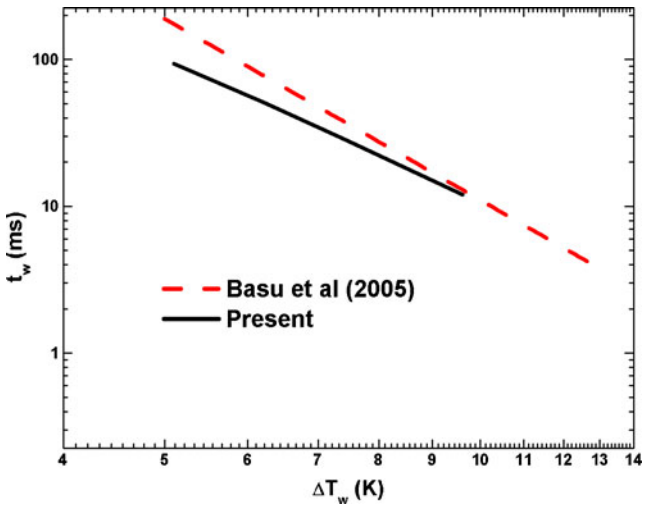

Fig. 6 Comparison between numerical results and experimental correlation for waiting time as a function of wall superheat. The simulations were carried out using a 1 mm thick copper disc at one atmosphere pressure

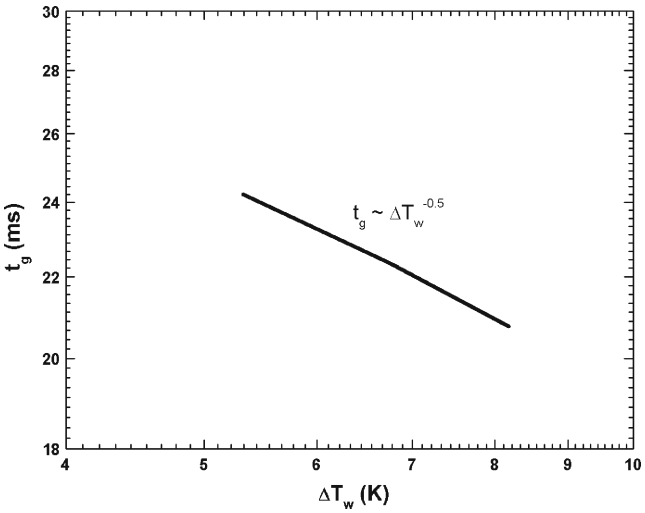

Fig. 7 Growth period as a function of wall superheat for water boiling on a 1 mm thick copper plate at one atmosphere pressure

experimentally by Myers et al. (2005) and numerically by Kunkelmann and Stephan (2010).

Figure 5 shows growth histories and waiting periods for two cases with different imposed heat fluxes and resulting average wall temperatures but otherwise identical conditions. As it has been shown numerically by Son et al. (1999), with increasing wall superheat the growth period decreases and the bubble departure diameter increases. However, a new and more discernible feature is the significant decrease in waiting periods for the same change in wall superheat.

Figure 6 shows that the waiting period can be related directly to the wall superheat when varying the heat flux boundary condition at the bottom of the solid and keeping all else unchanged. An increase in heat flux results in a higher average wall superheat and a smaller waiting period. The wall superheat reported was calculated in the same way as before by using Eq. 7. As seen in Fig. 6, an inverse power law is observed to fit well with the results obtained from a simple parametric study. The experimental correlation developed by Basu et al. (2005) for subcooled flow boiling corroborates this functional relationship. Similarly, Fig. 7 shows the effect of wall superheat on the growth period.

Table 2 Thermo-physical properties for different materials studied

	Glass	Steel	Copper
$k\ (W/m \cdot K)$	1.09	15	401
$\alpha \times 10^6\ (m^2/s)$	0.510	3.88	117

In Fig. 8, the effect of solid thickness on waiting time while a constant heat flux is applied at the base of the solid is shown. The results are shown for three solids with a fixed contact angle but widely varying thermo-physical properties as listed in Table 2. The behavior is similar for both steel and borosilicate glass: waiting time decreases as the wall thickness increases. This can be attributed to the fact that a thicker wall provides more thermal mass to aid in a quicker recovery of the surface temperature. As the thickness is increased further, the waiting time quickly attains an asymptotic value that becomes independent of thickness.

The main trend between the different materials in Fig. 8 is that with increasing thermal conductivity and diffusivity, the waiting time decreases. For the highly

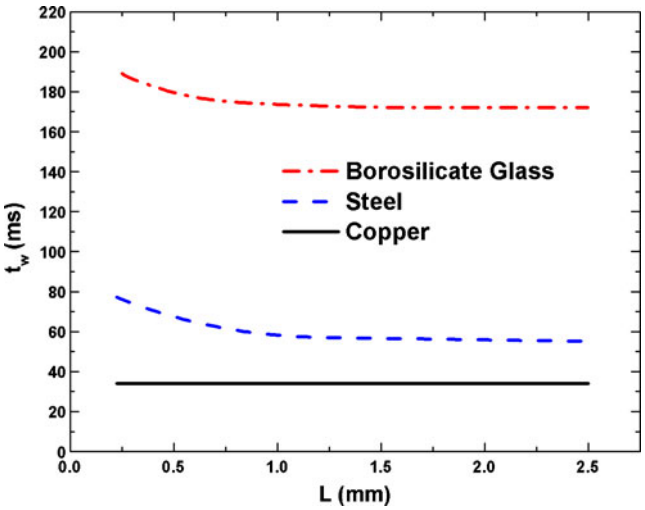

Fig. 8 Waiting time as a function of solid wall thickness for different materials with $q_{w,in} = 1.1$ W/cm^2 and $\Delta T_{ref} = 6$ K at one atmosphere pressure

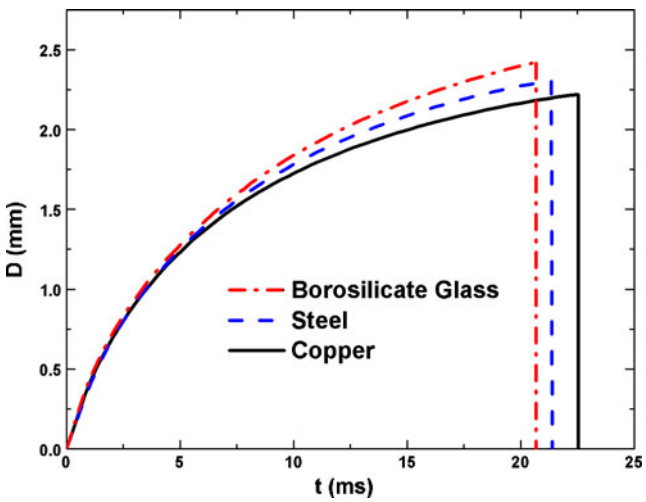

Fig. 9 Growth history for different wall materials with 0.3 mm wall thickness under identical conditions: $q_{w,in} = 1.1$ W/cm^2 and $\Delta T_{ref} = 6$ K at one atmosphere pressure

conductive copper, the time taken for the surface to recover its temperature is much smaller than it is for the thermally insulating borosilicate glass.

Figure 9 shows the bubble growth history for copper, steel, and borosilicate glass when quasi steady condition is achieved while keeping all other conditions unchanged. The wall thickness is 0.3 mm and the input heat flux is $q_w = 1.1$ W/cm^2. The clear pattern observed is that increasing wall thermal conductivity and diffusivity results in slower growth rates and smaller bubbles. Referring back to Fig. 8, we reiterate that improving wall thermal conductivity and diffusivity results in a shorter waiting period. One of the consequences of a shorter waiting period is that the thermal boundary layer has less time to develop before the next cycle begins. The boundary layer thickness and its effect on bubble growth can be seen on Fig. 10. If surrounded by a thinner thermal boundary layer, a bubble will grow

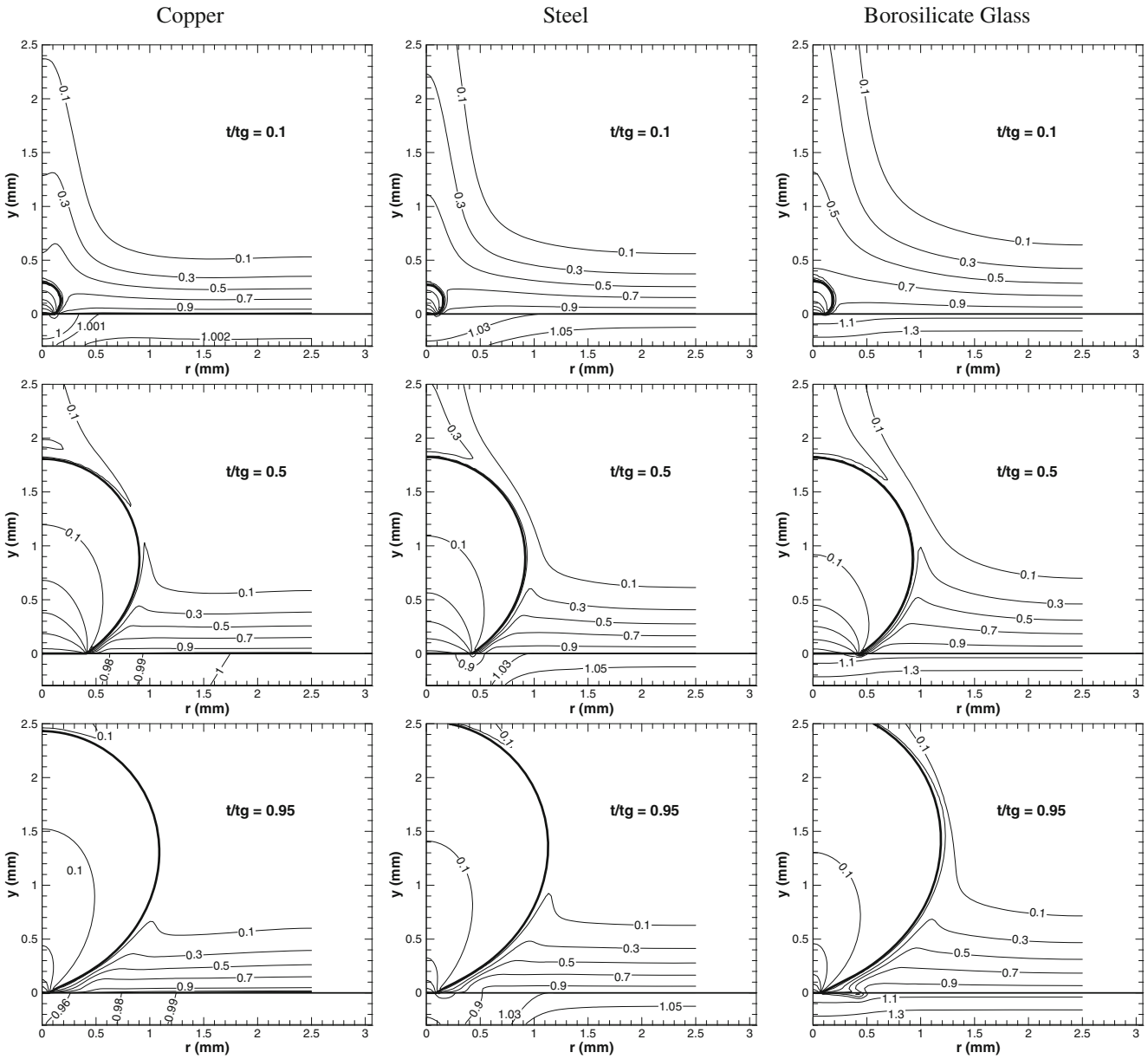

Fig. 10 Bubble growth and temperature contours for copper, steel, and borosilicate glass at nucleation, midway through the growth cycle, and right before departure. The phase interfaces are shown in bold. The input heat flux was $q_{w,in} = 1.1$ W/cm^2 and the reference wall superheat was $\Delta T_{ref} = 6$ K

more slowly than if surrounded by a thicker thermal boundary layer. Additionally, more heat transfer will take place directly from the solid wall to the liquid if the thermal layer is thinner. The first set of frames shows the bubble embryo shortly after nucleation and the temperature contours for copper, steel, and borosilicate glass. The temperature contours show clearly the difference in boundary layer thickness at nucleation for the different solid substrates. The second set of frames shows the bubbles approximately half way through the growth cycle, and the last set of frames shows the bubbles right before they depart. Right before departure, the size difference is noticeable, and so is the fact that for borosilicate glass which had the thickest boundary layer at nucleation, the bubble is still surrounded by superheated fluid even as it detaches from the wall.

Due to inertial effects, a higher growth rate affects the departure diameter. According to the correlation of Cole and Shulman (1966), for example, the departure

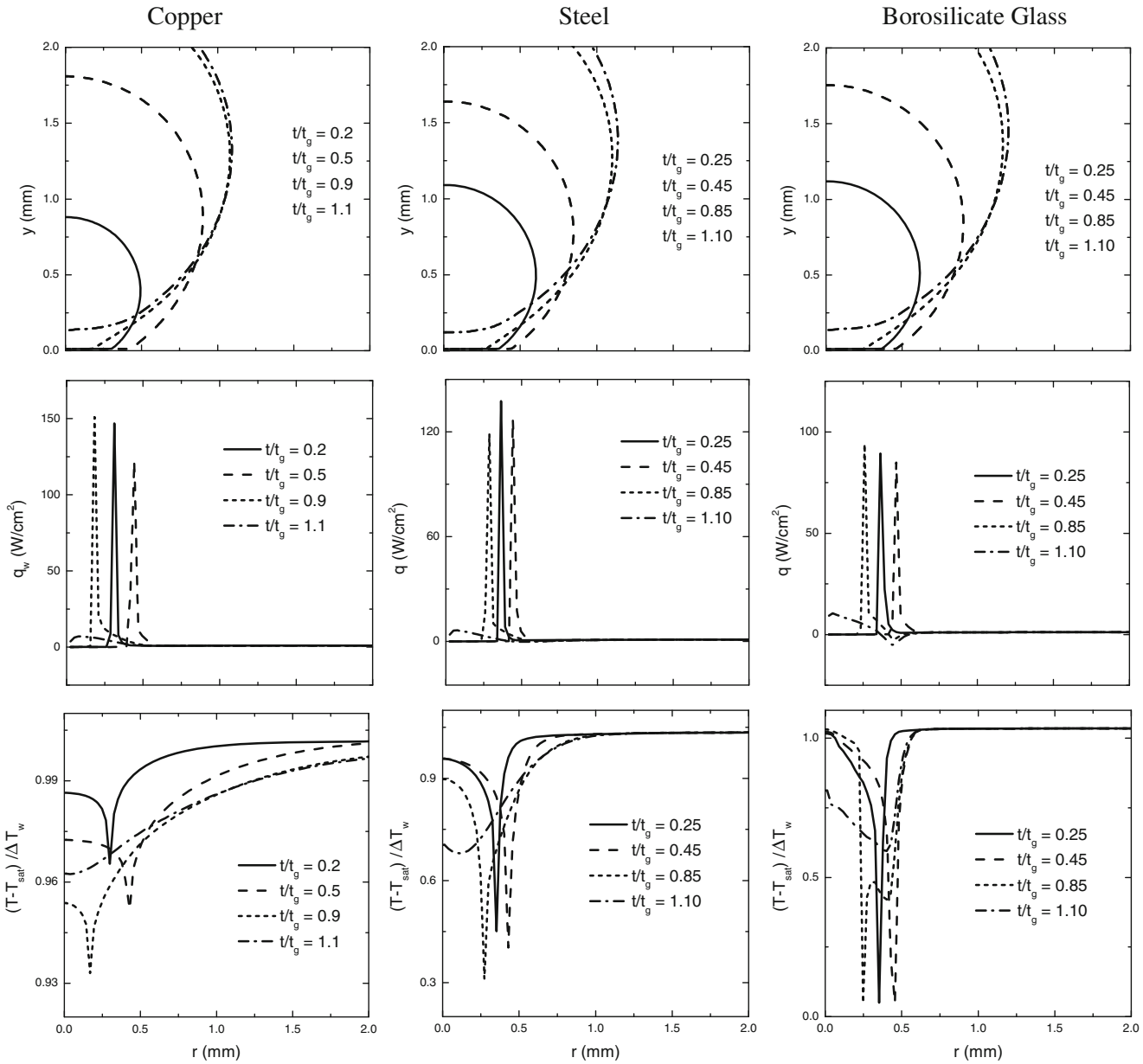

Fig. 11 Local wall superheat and heat flux as a function of radial location at different times during bubble growth and after departure for 0.3 mm copper, steel, and borosilicate glass. The input heat flux was $q_{w,in} = 1.1$ W/cm^2 and the reference wall superheat was $\Delta T_{ref} = 6$ K

diameter increases with increasing growth rate as is also observed in Fig. 9.

$$d_{Bd} = 0.0208\theta\sqrt{\frac{\sigma}{g\Delta\rho}}\left[1 + 0.0025\left(\frac{dd_B}{dt}\right)^{3/2}\right] \quad (8)$$

Figure 11 shows the local wall superheat and local wall heat flux as a function of the radial location at different times during bubble growth for copper, steel, and borosilicate glass. As the bubble grows and its base expands, the location where the rate of heat removal peaks moves radially out with the motion of the interface over the solid wall. The same is observed as the bubble base shrinks after reaching a maximum value.

The curves representing the surface temperature as a function of radius after departure show the absence of a sharp temperature drop in the absence of the evaporating microlayer during bubble growth. However, the less pronounced temperature drop affects a visibly larger surface area due to the liquid that rushes in to replace the bubble after departure. Quantitatively, the heat flux is of the order of 10^{-2} W/cm^2 where the solid is dry, 10^{-1} W/cm^2 where the solid is in contact with the superheated liquid boundary layer, and 10^2 W/cm^2 near the three phase point. During bubble growth, the actual peak heat flux can reach close to 150 W/cm^2 while the heat flux averaged over the entire surface of the disc remains at 1.5 W/cm^2. Due to the sharpness of the heat flux peak and its motion as time passes, any single location on the solid surface close to the cavity site will be exposed to abrupt temperature fluctuations as was also shown in Fig. 4.

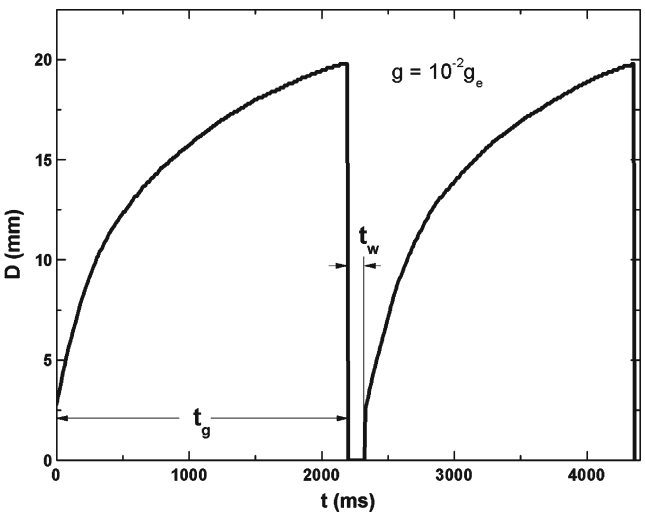

Fig. 12 The effect of gravity on growth and waiting times for water boiling on a 1 mm thick copper surface at one atmosphere pressure, $q_{w,in} = 0.36$ W/cm^2 with $\Delta T_{ref} = 6$ K

Figure 12 shows the growth history for water boiling on a 1 mm thick copper surface at one atmosphere pressure and reduced gravity, $g/g_e = 10^{-2}$. In comparison to the observations at Earth normal gravity, the growth period increases by two orders of magnitude and the departure diameter increases by one order of magnitude. However, the change in gravity only has second order effects on the solid substrate's recovery time. Therefore, the change observed in the waiting period (≈20 ms) is almost insignificant when compared to those of the growth period and departure diameter.

Conclusions

A complete numerical simulation of growing and departing bubbles on a horizontal surface has been carried out without any surface temperature or waiting time restrictions. The coupling of the solid thermal response to the simulation of nucleate boiling has provided for a more realistic description of the actual phenomena. Parametric studies have offered insight into the dependence of waiting time on wall superheat/heat flux, solid thickness, and thermo-physical properties of the solid.

- The time dependent heat flux distribution along the surface of the wall is found to vary by up to four orders of magnitude during bubble growth. It is highest near the triple point where microlayer evaporation takes place, and lowest near the center of the bubble base where the surface is dry. The same observations were made by Kunkelmann and Stephan (2010).
- Any given location on the solid surface that is traversed by the three-phase interline is seen to experience significant temperature fluctuations.
- The waiting time is found to decrease nonlinearly with increasing wall superheat and the behavior is similar to that proposed for flow boiling.
- Solid wall thickness and material properties are observed to affect waiting time significantly. Up to a limiting value, changing the heater thickness will affect the surface temperature recovery during nucleate boiling. Additionally, highly conductive materials are able to recover faster than poorly conductive materials.
- As gravity is reduced, the bubble growth period increases at a much faster rate than the waiting period between successive bubbles.

Acknowledgements This work received support from the National Aeronautics and Space Administration (NASA) under the Flight Experiment Program.

References

Basu, N., Warrier, G.R., Dhir, V.K.: Wall heat flux partitioning during subcooled flow boiling: Part 1—model development. J. Heat Tran. **127**, 131–140 (2005)

Cole, R., Shulman, H. L.: Bubble growth rates at high Jakob numbers. Int. J. Heat Mass Tran. **9**, 1377–1390 (1966)

Douglas, J., Gunn, J.: A general formulation of alternating direction methods. I. Numer. Math. **6**, 428–453 (1964)

Guo, Z., El-Genk, M.S.: Liquid microlayer evaporation during nucleate boiling on the surface of a flat composite wall. Int. J. Heat Mass Tran. **37**, 1641–1655 (1994)

Han, C.Y., Griffith, P.: The mechanism of heat transfer in nucleate pool boiling, Part I. Bubble initiation, growth and departure. Int. J. Heat Mass Tran. **8**, 887–904 (1965)

Hsu, Y.Y., Graham, R.W.: An analytical and experimental study of the thermal boundary layer and ebullition cycle in nucleate boiling. NASA TND-594 (1961)

Hsu, Y.Y., Graham, R.W.: Transport Processes in Boiling and Two-Phase Systems. American Nuclear Society, La Grange Park, IL (1986)

Kunkelmann, C., Stephan, P.: Modification and Extension of a Standard Volume-of-Fluid Solver for Simulating Boiling Heat Transfer. Proc. 5th European Conference on Computational Fluid Dynamics ECCOMAS CFD2010, Lisbon, Portugal (2010)

Kunkelmann, C., Stephan, P.: Numerical simulation of the transient heat transfer during nucleate boiling of refrigerant HFE-7100. Int. J. Refrigeration **33**, 1221–1228 (2010)

Lay, J.H., Dhir, V.K.: Shape of a vapor stem during nucleate boiling of saturated liquids. J. Heat Tran. **117**, 394–401 (1995)

Magrini, U., Nannei, E.: On the influence of the thickness and thermal properties of heating walls on the heat transfer coefficients in nucleate pool boiling. J. Heat Tran. **97**, 173–178 (1975)

Mann, M., Stephan, K., Stephan, P.: Influence of heat conduction in the wall on nucleate boiling heat transfer. Int. J. Heat Mass Tran. **43**, 2193–2203 (2000)

Moore, F.D., Mesler, R.B.: The measurement of rapid surface temperature fluctuations during nucleate boiling of water. AIChE. J. **7**, 620–624 (1961)

Myers, J.G., Yerramilli, V.K., Hussey, S.W., Yee, G.G., Kim, J.: Time and space resolved wall temperature measurements during nucleate boiling with constant heat flux boundary conditions. Int. J. Heat Mass Tran. **48**, 2429–2442 (2005)

Son, G., Dhir, V.K., Ramanujapu, N.: Dynamics and heat transfer associated with a single bubble during nucleate boiling on a horizontal surface. J. Heat Tran. **121**, 623–632 (1999)

Son, G., Dhir, V.K., Ramanujapu, N.: Numerical simulation of bubble merger process on a single nucleation site during pool nucleate boiling. J. Heat Tran. **121**, 623–632 (2002)

Wang, C.S., Dhir, V.K.: Effect of surface wettability on active nucleation site density during pool boiling of water on a vertical surface. J. Heat Tran. **115**, 659–669 (1993)

Wang, C.S., Dhir, V.K.: On the gas entrapment and nucleation site density during pool boiling of saturated water. J. Heat Tran. **115**, 670–679 (1993)

Yoon, H.Y., Koshizuka, S., Oka, Y.: Direct calculation of bubble growth, departure, and rise in nucleate pool boiling. Int. J. Multiphas Flow **27**, 277–298 (2001)

Zeng, H., Zhu, J.: An efficient ADI algorithm for solving 3-D convection diffusion equations with Neumann boundary conditions. International Conference on Parallel Processing Workshops, pp. 320–326 (2002)